

Using shipping noise for sound speed inversion in coastal areas

Ana Bela Santos, Paulo Felisberto, Sérgio M. Jesus
LARSyS, Universidade do Algarve
8005-139 Faro, Portugal
Email: {absantos, pfelis, sjesus}@ualg.pt

Abstract—Passive sound speed estimation using radiated ship noise is an appealing approach for long-term ocean observation close to ship lanes. In this paper we analyze the noise recorded in two drifting vertical line arrays (VLAs) deployed 1 km apart, in Setúbal’s underwater canyon area off the west coast of Portugal during the RADAR’07 sea trial. Automatic Information System (AIS) recordings for this period reveal a major tanker passing in the area, with its acoustic signature observed in the spectrogram as a characteristic striation time-frequency pattern. By cross correlation and beamforming of the received signals at the VLAs we obtain propagating paths traversing the hydrophones of both VLAs and respective travel times. Such information is used for sound speed estimation. We discuss the applicability of the method to track sound speed perturbations using historical sound speed profiles for the area obtained from CMEMS (COPERNICUS Marine Environment Monitoring Service). This work is a contribution for application in a passive ocean acoustics framework for the estimation of sound speed perturbations in the water column.

Index Terms—Passive inversion methods, passive ocean acoustic tomography, shipping noise.

I. INTRODUCTION

Passive ocean acoustic tomography exploits opportunistic noise sources (e.g. ambient noise or anthropogenic noise) to infer physical features of the ocean. Commercial shipping noise is the main source of anthropogenic acoustic noise in the ocean in the low frequency band (10 to 500 Hz) [1]. The radiated shipping noise spectra is characterized by a few low discrete frequency tones superimposed on a diffuse background pedestal [2]. It is well known that low frequency acoustic waves propagate efficiently through the ocean sound channel, this causes shipping noise to propagate over long distances and be present nearly everywhere. Further, the structure of ocean noise is determined by the environment, namely water column parameters; which justifies the application of shipping noise in acoustic tomography. The broadband noise radiated by a moving ship creates a characteristic signal when recorded on a single receiver. In the time-frequency domain, the received signal presents an interference pattern also known as striation pattern. This pattern is the combination of three important factors: the source is mobile, broadband and radiating in a shallow water environment [3]. The filtered noise cross correlation between the VLAs of sensors and posterior ensemble average enables the coherent wave front structure extraction [4], [5]. Subsequent beamforming enhances the spatio-temporal properties of the propagating field between the two

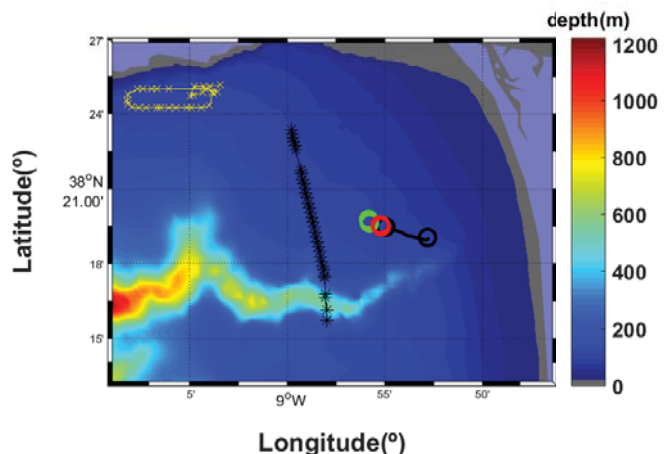


Fig. 1. RADAR’07 July, 13th GPS estimated position of the two VLAs (in red and green circles) and the NRP D. Carlos I track in black, imposed on a bathymetric map of the region complemented with AIS information data, during 1h period.

VLAs. In this work we use the above method to obtain angles and travel times estimates between the two VLAs. Provided with this information, a similar structure for the sound speed profiles of interest in the region is considered. From a historical series of CTD casts in the area, the propagating field between the VLAs is simulated using the same structural information (angles and associated rays) and perturbed times are extracted. The usage of a tomography travel time method is considered to obtain inverted sound speed profiles and the associated error estimate. The results show that synthetic inverted sound speed profiles are in reasonable agreement with summer and winter sound speed profiles. This paper is organized as follows: Section II describes briefly the sea trial campaign where the data was acquired; section III discusses the time difference of arrival and angle of arrival estimation from noise cross-correlation; section IV discusses the results of sound speed inversions performed with a ray propagation model under three different scenarios and section V draws some conclusions.

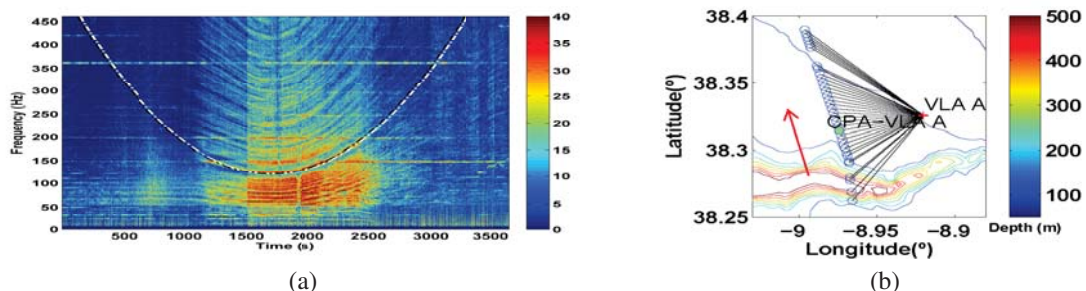


Fig. 2. (a): Recorded radiated noise spectrogram from 10h50m to 11h50m of July, 13th. (b): AIS estimated track zoom represented by the blue circles and the closest point of approach (CPA) to the VLA A represented by a green dot, superimposed on an isobathymetric plot.

II. OVERVIEW OF THE RADAR'07 SEA TRIAL

The RADAR'07 experiment took place from 9 to 15 July, 2007, in the continental platform, off the Portugal west coast near the town of Setúbal, approximately 50 km south from Lisbon and involved the oceanographic ship NRP D. Carlos I, from the Portuguese Navy. The data collected included active acoustic data covering a wide band from 500 Hz up to 15 kHz, received on the three vertical arrays and used for network tomography as well as for high-frequency tomography and underwater acoustic communications [6]. The two VLAs considered in this work, VLA A and VLA B, have 16 and 8 sensors, respectively. VLA A has 16 sensors equally spaced from 6 to 66 m depth and VLA B has 8 sensors two at 9 and 14 m, and the other six are equally spaced from 54 to 79 m depth. In this work we analyze a period of one hour of Julian Day 194 (13th of July). Figure 1 shows the geometry for that specific period and the AIS information for vessels in the area where estimated track of a major tanker is depicted (in black *). The estimated distances from the tanker to VLA B and VLA A vary respectively from 4.1 to 6.1 km and 4.8 to 7.1 km.

III. TIME DIFFERENCE AND ANGLE OF ARRIVAL ESTIMATION

We selected acoustic data sets acquired in both VLAs from 10h 50m to 11h 50m of July 13th for shipping noise processing, due to the AIS information on the major tanker in the area. The received signals were 30 - 460 Hz bandpass filtered to enhance, since active signals were transmitted above 500Hz. Figure 2(a) shows the spectrogram of the received radiated shipping noise at one sensor of one of the VLAs and Figure 2(b) depicts the estimated AIS tanker track and closest point of approach to VLA A superimposed on the isobathymetric plot of the region. The acoustic signature of the tanker is very clear, with a time-frequency striation pattern and a superimposed parabola for the theoretical waveguide invariant ($\beta \approx 1$). The transition from the Setúbal canyon to the shallow water environment is also depicted through the lack of the striation pattern before 1200s (minute 20) of the recordings as the ship crosses the canyon upward to the port as can be observed in Figure 2(b).

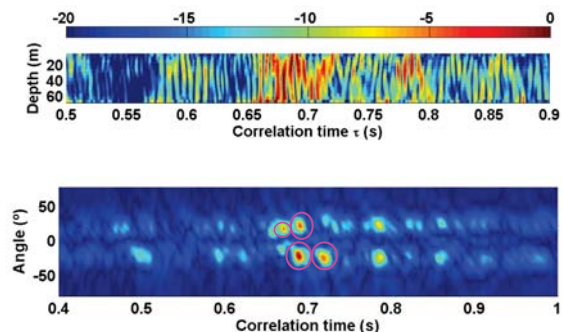


Fig. 3. (a): Wave front obtained from 7 min time series when the 2 VLAs are aligned with the tanker; (b): Direction of arrival estimation from common ray paths and selection of high intensity angle amplitudes/travel times.

Figure 3(a) presents the wave front obtained from averaged cross correlated data between sensor 3 of VLA B and all sensors of VLA A, using one minute correlation window, with 59 s overlap. It depicts the traveling wave fronts as if they were emanating from sensor 3 of VLA B to all sensors of VLA A. Regarding the cross correlation method, a time series of 7 minutes is considered, time centered at the closest point of approach (CPA), when both VLAs are aligned with the major tanker as can be observed in Figures 1 and 2(b). Figure 3(b) presents the beamforming results of the data presented in Figure 3(a). Using the cross correlation procedure as shown in Figure 3(a) for all VLB sensors and all VLA sensors, 8 wave fronts were obtained. By time domain beamforming of the 8 obtained wave fronts (as in Figure 3(b)), a series of time differences of arrival and angles of arrival estimates were obtained. This series of peak values was consistent for all the 8 analyses performed revealing 4 amplitude angles of 22.2, -22.2, -24.5 and 19.8 degrees, respectively and corresponding arrival times differences. This spatial filtering technique from shipping noise enabled the angles and amplitudes of the propagating paths common to both VLAs and corresponding travel times, features of major importance for sound speed inversion from a geometric acoustics perspective [7], [8].

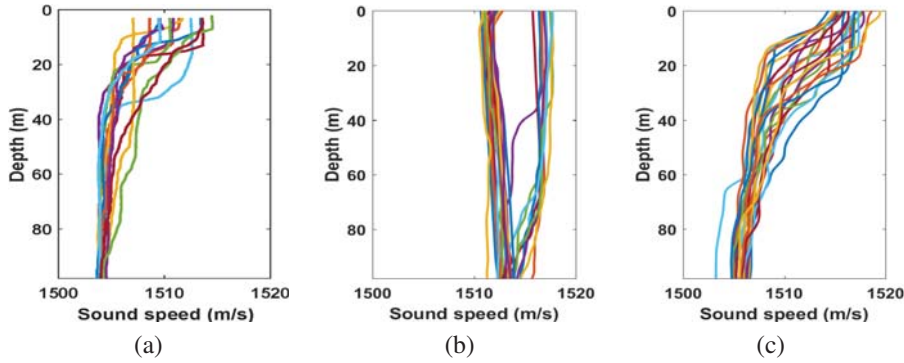


Fig. 4. Sound speed profiles obtained from: (a) CTD casts during RADAR'07 experiment; (b) (c) winter and summer historical profiles [12].

IV. SOUND SPEED INVERSION

Having obtained angle and travel time estimates in the previous section, we consider the passive travel time based tomography to invert the perturbed sound speed profiles.

A. Methodology

The travel times perturbation can be written in terms of a linear system as

$$\delta\tau = \mathcal{E}\alpha + \mathbf{n} \quad (1)$$

with $\mathcal{E} = \mathbf{E}\mathbf{H}$ and \mathbf{n} is the noise term, \mathbf{E} is the observation matrix which combines the perturbation of the the sound speed and travel times, $\delta\mathbf{c} = \mathbf{H}\alpha$ is the sound speed perturbation, regularized in terms of Empirical Orthogonal Functions (EOFs), where \mathbf{H} stands for the EOFs considered and α are the corresponding coefficients [7], [9]. The number of EOFs is selected according to an empirical rule, representing at least 80% of the total variability in measured sound speed profiles [10]. The solution to this problem in the least squares sense, or Least Squares Estimator is:

$$\hat{\alpha} = (\mathcal{E}^T \mathcal{E})^{-1} \mathcal{E}^T \delta\tau \quad (2)$$

obtained according to the minimization of the cost function, or LS error [11].

$$J_{\min} = \delta\tau^T \left(\mathbf{I} - \mathcal{E} (\mathcal{E}^T \mathcal{E})^{-1} \mathcal{E}^T \right) \delta\tau \quad (3)$$

where superscript T stands for the transpose operator. The estimator can be obtained through a single inversion for a single sensor pair. In this work, 2 VLAs of sensors are considered, thus the method could be expanded to consider all sensor pairs. Yet, since know prior information is assumed relating sensor positions, considering separate sensor pairs allows the minimization criteria to be applied separately, discard outliers if they are present and average the final result, obtaining as such, a spatially integrating measure for the estimator.

B. Results and Discussion

Figure 4 presents three panels of sound speed profiles, on the left a series of sound speed profiles obtained from CTD casts at the location of RADAR'07, the other two panels present historical series of local sound speed profiles obtained

from CMEMS data base [12], representative of winter and summer profiles (Figure 4(b) and (c)). These CTD casts were the basis for synthetic inversions taking into account a limitation in the propagating aperture angle space to $[-28, 28]$ degrees interval, obtained with the ray tracing model TRACEO [13]. The chosen interval takes into account the values obtained from beamforming procedure described in Section III. The environment is considered range independent with a 98 m depth water column, above a sediment half-space, with bottom parameters compressional velocity $c_p = 1650$ m/s, compressional attenuation $\alpha_p = 0.8$ dB/ λ and density $\rho = 1.9$ g/cm³ [6]. We consider all possible 128 sensor pairs configurations with horizontal distance of 950 m, in agreement with the setup presented in Figure 1. For each sensor pair configuration, a set of four eigenrays is selected in close agreement with values obtained by the previously method of section III. To obtain the perturbed travel times we consider the regularization of the summer CTDs using 3 EOFs, and two EOFs for the winter CTDs, since in winter CTDs, two EOF already represent 96% of the associated variability in sound speed profiles. From the perturbed travel times obtained, the average inverted sound speed is obtained according to Eq. (3) and conditioned to obey a Chebyshev threshold $k = \sqrt{10\text{var}(\mathbf{J})}$, where \mathbf{J} are the LS errors for all the inverted sound speed profiles. That is, if $J > k$ then the inverted sound speed for the pair is discarded. Figure 5 depicts illustrative cases of synthetic inverted sound speed profiles: in the upper panel, inverted sound speed profiles from RADAR'07 regularized CTDs, in the middle panel, inverted sound speed profiles from regularized CMEMS historical summer CTDs and in the lower panel, inverted sound speed profiles from regularized CMEMS historical winter profiles. In all representations a composite of the mean sound speed profile (in blue), perturbed sound speed profile (in black) and inverted sound speed profile (in red) is represented. The values of the associated root mean squared error between the perturbed and inverted sound speed profiles are: (a) 0.18 m/s; (b) 0.26 m/s; (c) 0.49 m/s; (d) 0.72 m/s; (e) 0.56 m/s; (f) 0.38 m/s; (g) 0.52 m/s; (h) 0.08 m/s and (g) 0.21 m/s respectively. Overall it can be observed that in some cases the obtained

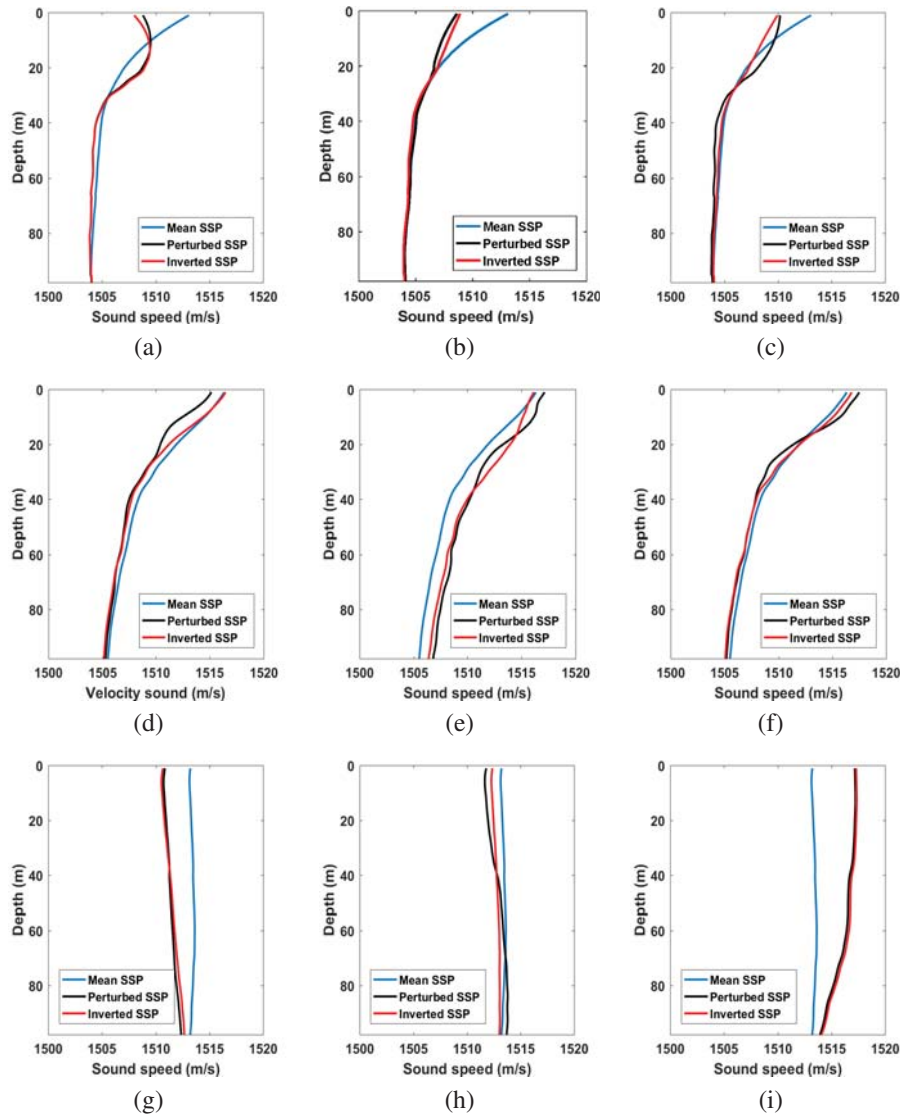


Fig. 5. Inverted Sound Speed Profiles obtained from: (a,b,c) CTD casts during RADAR'07 experiment; (d,e,f) summer historical profiles; (g,h,i) winter historical profiles.

inversions present good agreement results, while in some cases the inversion doesn't adjust very well to the perturbed sound speed profile, although in most cases the trend is followed. In order to describe the global behavior of the inverted sound speed profiles, Figure 6 shows the histogram of the root mean squared errors for all 128 the simulations performed. It can be observed that more than 2/3 of the inverted sound speed profiles have an associated root mean squared error less than 0.4 m/s. This approach, although suitable to optimization will be considered for future application with real acoustic data.

V. CONCLUSIONS

In this work we have addressed the usage of ships of opportunity to obtain coherent information and travel times from the propagating paths between two VLAs in a coastal area. Moreover, historical sound speed profiles usage for

synthetic inversion of sound speed profiles was also addressed, providing some preliminary results that suggest the feasibility of the method for future application in a passive ocean acoustics tomography framework to the estimation of sound speed perturbations in the water column, obtained from shipping noise recordings.

ACKNOWLEDGMENTS

This work has been conducted using E.U. Copernicus Marine Service Information and was partially funded by projects SUBECO under the PO-Navy research program and by the H2020 European Research Program under project EMSODEV (contract 676555).

REFERENCES

- [1] J. A. Hildebrand, "Anthropogenic and natural sources of ambient noise in the ocean," *Mar. Ecol. Prog. Ser.*, vol. 395, pp. 5–20, 2009.

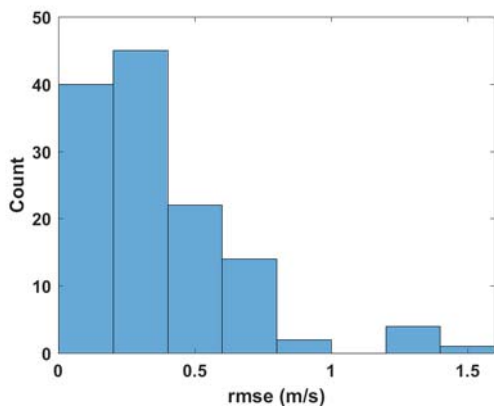


Fig. 6. Histogram of the root mean squared error associated to the inverted sound speed profiles.

- [2] R. J. Urick, *Principles of Underwater Sound 3rd Edition*. Peninsula Pub, Aug. 1996.
- [3] C. Gervaise, B. G. Kinda, J. Bonnel, Y. Stéphan, and S. Vallez, "Passive geoacoustic inversion with a single hydrophone using broadband ship noise," *The Journal of the Acoustical Society of America*, vol. 131, no. 3, pp. 1999–2010, 2012. [Online]. Available: <http://dx.doi.org/10.1121/1.3672688>
- [4] A. B. Santos, P. Felisberto, and S. M. Jesus, "Acoustic channel frequency response estimation using sources of opportunity," in *2016 IEEE/OES China Ocean Acoustics (COA)*, Jan 2016, pp. 1–4.
- [5] S. W. Lani, K. G. Sabra, W. S. Hodgkiss, W. A. Kuperman, and P. Roux, "Coherent processing of shipping noise for ocean monitoring," *The Journal of the Acoustical Society of America*, vol. 133, no. 2, pp. EL108–EL113, 2013.
- [6] C. Soares, S. M. Jesus, P. Hursky, T. Folegot, C. Martins, F. Zabel, L. Quaresma, D.-S. Ko, and E. F. Coelho, "Random array of drifting acoustic receivers (radar'07)," Universidade do Algarve, Faro, Portugal, Internal Report Rep 04/07, December 2007.
- [7] W. Munk, P. Worcester, and C. Wunsch, *Ocean Acoustic Tomography*. Cambridge University Press, 1995.
- [8] O. C. Rodriguez and S. M. Jesus, "Physical limitations of travel-time-based shallow water tomography," *The Journal of the Acoustical Society of America*, vol. 108, no. 6, pp. 2816–2822, 2000.
- [9] S. Salon, A. Crise, P. Picco, E. de Marinis, and O. Gasparini, "Sound speed in the mediterranean sea: an analysis from a climatological data set," *Annales Geophysicae*, vol. 21, no. 3, pp. 833–846, 2003. [Online]. Available: <http://www.ann-geophys.net/21/833/2003/>
- [10] S. M. Jesus, C. Soares, E. Coelho, and P. Picco, "An experimental demonstration of blind ocean acoustic tomography," *The Journal of the Acoustical Society of America*, vol. 119, no. 3, pp. 1420–1431, 2006.
- [11] S. M. Kay, *Fundamentals of Statistical Signal Processing, Volume I: Estimation Theory*. Prentice Hall, 1993.
- [12] (2017, January) COPERNICUS Marine Environment Monitoring Service. [Online]. Available: <http://www.copernicus.eu>
- [13] O. C. Rodriguez, *The TRACEO ray tracing program*, <http://www.siplab.fct.ualg.pt/models.shtml>, date last viewed 3/05/15.